Journal of Dentistry 164 (2026) 106254

Contents lists available at ScienceDirect

Journal of Dentistry

journal homepage: www.elsevier.com/locate/jdent

Accuracy of full-arch implant scan with Nexus IOS® scan gauges versus different conventional scan bodies: An in vitro comparative study

Henriette Lerner [a,*], Paul Weigl [a], Robert Sader [a], Michael Klein [b], Mariano A. Polack [c], Frank J. Tuminelli [d,e]

[a] Academic Teaching and Research Institution of Johann Wolfgang Goethe-University, Frankfurt am Main, Germany
[b] Private Practice, Cedarhurst, NY, USA
[c] Private Practice, Gainesville, VA, USA
[d] American Board of Prosthodontics, Graduate Prosthodontics VA NY Harbor Healthcare System, Adjunct Clinical Instructor, NYU Dental School, NY, NJ, USA
[e] Hofstra Northwell School of Medicine, USA

ARTICLE INFO

Keywords:
Intraoral scanners
Dental implants
Full-arch implant impression
In vitro, trueness
Precision

ABSTRACT

Objective: To evaluate the accuracy of full-arch (FA) implant scan with a novel system (Nexus IOS®, Osteon Medical) using scan gauges (SGs), and to compare it with that of different conventional scan body (SB) systems that are currently available.
Methods: A plaster model with 4 multi-unit-abutment analogs was prepared and inter-implant distances between its analogs were measured using a coordinate measuring machine (CMM), to obtain reference distances. An expert operator used an intraoral scanner (IOS) to capture scans with five different systems (Nexus IOS®, DESS®, Medentika®, IPD® and Elos®, $n = 10$ scans per group). These measurements were compared with the reference CMM-generated model to calculate inter-implant distance trueness. The study design addressed three questions: 1) Are there overall differences among the systems? 2) Are there overall differences among segments/points? and 3) For a given segment did systems perform differently? A statistical analysis was performed.
Results: Among the systems, Nexus IOS® system exhibited the highest trueness, followed by DESS®. Medentika® and IPD® showed slightly higher deviations and variability, indicating moderate performance. Elos® had the least trueness among the systems tested, with the highest median deviation and the widest overall spread, suggesting greater inconsistency in dimensional accuracy.
Conclusions: Within the limitations of this *in vitro* study, the Nexus IOS® SGs demonstrated the highest dimensional accuracy, showing superior trueness and precision in FA implant scanning compared with conventional SBs.
Statement of clinical relevance: These findings support the potential of calibrated SGs to improve digital FA implant accuracy and consistency, aligning with emerging literature on calibrated and framework-based scanning approaches.

1. Introduction

Intraoral scanners (IOSs) have revolutionized prosthodontics by simplifying the implant prosthetic workflow, making it more efficient and predictable [1–3]. IOSs provide sufficient accuracy for the digital design and fabrication of restorations through computer-assisted design (CAD) and computer-assisted manufacturing (CAM) systems such as milling machines and three-dimensional (3D) printers, enabling the production of clinically precise fixed restorations from various materials [4,5]. Numerous clinical studies have confirmed predictable accuracy for short-span prostheses, including single crowns (SCs) [6–10] and fixed partial dentures (FPDs) [11–13], when designed and fabricated using intraoral scans and CAD/CAM workflows.

However, the use of IOSs in completely edentulous patients remains a topic of debate both clinically and in the scientific literature [14–17]. Several studies and systematic reviews indicate that IOSs still lack the accuracy required for fabricating implant-supported full-arch fixed dental prostheses (ISFDPs) with clinically acceptable precision [15,16].

* Corresponding author.
E-mail addresses: h-lerner@web.de (H. Lerner), weigl@em.uni-frankfurt.de (P. Weigl), sader@em.uni-frankfurt.de (R. Sader), mkdds@optonline.net (M. Klein), mpolack@me.com (M.A. Polack), prosthodoc@aol.com (F.J. Tuminelli).

https://doi.org/10.1016/j.jdent.2025.106254
Received 5 November 2025; Received in revised form 12 November 2025; Accepted 18 November 2025
Available online 19 November 2025

This limitation is primarily attributed to stitching errors inherent to intraoral scanning and the intrinsic accuracy of the specific IOS used [18,19]. Many additional variables influence the quality of full-arch optical impressions, including operator skill, scanning strategy [20], and characteristics of the scan bodies (SBs)—such as geometry, material, and dimensional tolerances [21,22]. Other relevant factors include the number, position, angulation, and inter-implant distance [23], environmental conditions like light and temperature [24], and the congruence between the SB mesh and its CAD library counterpart [25,26].

Controlling all these factors can lead to clinically accurate ISFDPs produced through a fully digital workflow [20], yet doing so remains challenging for clinicians. Consequently, various alternative approaches have been proposed, including solid indexes (SIs) [27–29], auxiliary systems (ASs) [30–32], SB connection systems [33,34], extraoral photogrammetry (EPG) [35], and, more recently, intraoral photogrammetry (IPG) [36,37]. SIs require no financial investment but are analog rather than digital procedures [29]. ASs represent a valid digital solution but necessitate two separate intraoral scans—one for designing the auxiliary device and another for scanning with it in place [32]. Splinting SBs may not consistently improve accuracy: while some studies report enhanced trueness [33], others suggest that it primarily affects scanning speed and regularity rather than reducing stitching errors [34]. Although *in vitro* results cannot be directly extrapolated to clinical conditions, faster scanning may limit mesh distortion and improve congruence with implant libraries, thereby reducing superimposition errors [25,26].

EPG has demonstrated high precision in registering implant positions for ISFDP fabrication but requires costly equipment and an additional step to merge photogrammetric and intraoral data [35]. IPG simplifies the process but is currently supported only by the Elite IPG® IOS (Shining 3D, Hangzhou, China) [36,37].

An alternative system, NEXUS IOS® (Osteon Medical, Keystone Dental Group, Melbourne, Australia), employs modular horizontal scan gauges (SGs) of various shapes, lengths, and heights, differing from conventional vertically oriented SBs. Manufactured from grade 5 titanium, SGs are resistant to sterilization-induced distortion, ensuring precision and durability [38]. They are secured to multiunit abutments (MUAs) compatible with major implant systems [38]. By creating slight horizontal overlaps between adjacent SGs, this design allows for faster, continuous scanning, improving accuracy across inter-implant spans [39].

Each Nexus IOS® SG is linked to a dedicated CAD library generated by direct probing of its physical counterpart, eliminating manufacturing tolerances and ensuring a precise match between physical and digital components [38]. In contrast, conventional SBs rely on mass-produced universal CAD libraries, which introduce dimensional discrepancies from fabrication variability [38,39]. In a multicenter retrospective study, Klein et al. [40] evaluated 37 ISFDPs fabricated from intraoral scans using the Nexus IOS® system in 29 patients across six centers. Over a three-year period, the authors assessed marginal fit, functional and esthetic integration, implant survival, and biologic and prosthetic complications, reporting 100% implant survival and minimal complications at one year [40]. All ISFDPs were clinically acceptable upon insertion [40].

The aim of this *in vitro* study was to evaluate the accuracy of FA implant scans obtained with Nexus IOS® SGs and compare them with conventional SBs currently used in clinical practice.

2. Materials and methods

2.1. Reference model and precision probing

A type IV plaster reference model (RM) was prepared with 4 MUA analogs (Nobel Biocare, Kloten, Switzerland) positioned at a standard distance and an axial clearance around the abutments of approximately 3 mm. A reference for measurement of the RM was created using a coordinate measuring machine (CMM), by indirectly probing the MUA analogs. The indirect assessment was done using a precision-made cylinder (PMC), which was manufactured to 5-micron precision. Each measurement was repeated 5 times, and each time the cylinders were unscrewed and re-screwed between each measurement. The positional output of all 5 measurements was compared, and a mean control number was established. This mean control number was used as a Reference, representing the RM.

2.2. Scanning groups

After capturing the RM by precision probing, an expert operator with over 10 years of experience in intraoral scanning used the same IOS (i-700®, Medit, Seoul, South Korea), to capture the scans of the different SBs. The IOS was calibrated before starting the scanning process, by using the calibration devices according to the protocol advised by the manufacturer. A total of 5 SB systems were chosen for this study and this formed the 5 scanning groups. The scans adopt a specific strategy (which included a progressive zig-zag movement, from right to left and back) using different types of SBs in each group:

- *Group 1*: SGs by Nexus IOS® (Osteon Medical, a Keystone Dental Group company, Melbourne, Australia) (Fig. 1**A,B**). https://www.nexusios.com/scan-gauges
- *Group 2*: DESS Intraoral SB on Multiunit RP 52.007® (DESS Dental Smart Solutions, Barbera del Valles, Barcelona, Spain) (Fig. 2**A**) https://www.dess-usa.com/intraoral-scan-body-on-multiunit-rp-52–007/
- *Group 3*: Medentika 8500 Multi-Unit SB® (Medentika GmbH, a Straumann Group, Hügelsheim, Germany) (Fig. 2**B**) https://shop.straumann.com/medentika/di/en_di/Prosthetics-by-product-type/Prosthetic-Accessories/Scanbodies/C-Serie-Multi-unit-scanbody-straight/p/C%208500/
- *Group 4*: Elos Accurate Intra Oral Position Locator Kit Multi-unit Abutment NP/RP IO 2C-A® (Elos, Gothenburg, Sweden) (Fig. 2**C**) https://store.nobelbiocare.com/au/en/cad-cam/open-access-components/intraoral-components/elos-accurate-intra-oral-position-locator-multi-unit-abutment-np-rp-1
- *Group 5*: IPD/AB-SR-01 SB® (IPD Dental, Matarò, Barcelona, Spain) (Fig. 2**D**) https://ipd2004.com/en/nobel-biocare-multi-unit-scan-abutment-intra-oral.

For group 1, the SGs were screwed onto the MUAs, ensuring that they were placed close to each other, forming an arch, reducing the distances existing between the fixtures, but without contact between the SGs. The SGs were captured in full, with their alignment guiding the scan path utilized by the operator during the execution of the scan. The scans were conducted in a sequence of two consecutive scans, one from left-to-right and then right-to-left over the same gauge arrangement, forming one set of scans. This approach was taken according to the specification of Nexus IOS for adequate accuracy of the system. A total of 10 sets of scans (2 scans per set) were captured for group 1.

For the other groups (Group 2, 3, 4 and 5) the same operator screwed the SBs onto the MUAs using the proprietary drivers, and scanned the RM, following the same scanning strategy, for a total of 10 IOS scans per group.

2.3. Outcome evaluation

The 10 Nexus IOS® scan sets were sent to Osteon for 3D processing, where the scans in the set were merged, serving as a comprehensive 3d representation of each scan set data. The resulting output file was further aligned with the corresponding library of the scan gauge kit. The specific library contained the geometric references specific to the kit (IOS_AA_20,494). Once the alignment with the library was complete, the final output file was generated, containing the detailed 3D positional

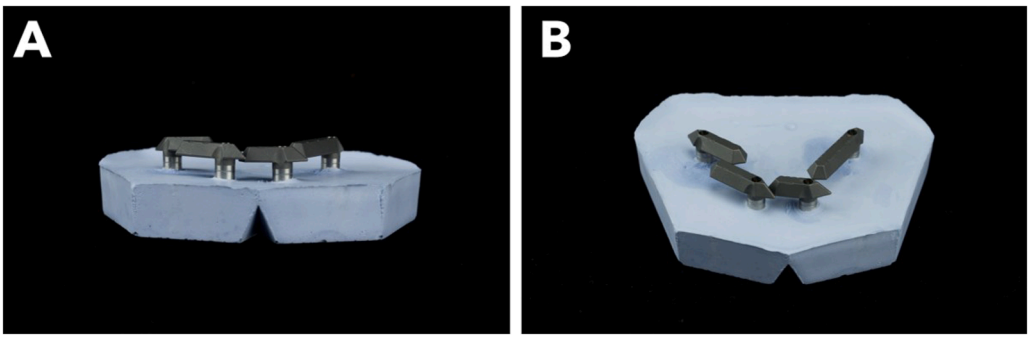

Fig. 1. The SGs by Nexus IOS® (Osteon Medical, a Keystone Dental Group company, Melbourne, Australia) in position: (A) Frontal view; (B) Occlusal view.

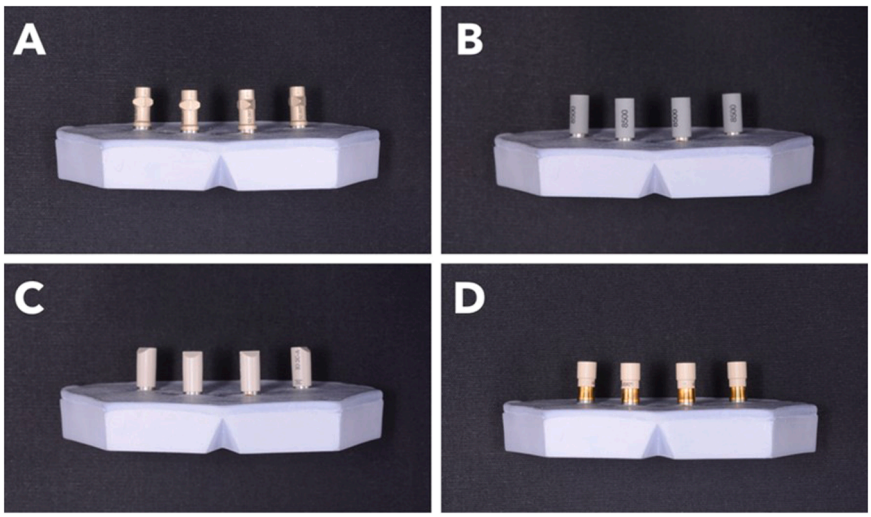

Fig. 2. The reference model with the different SBs in position: A) DESS Intraoral SB on Multiunit RP 52.007® (DESS Dental Smart Solutions, Barbera del Valles, Barcelona, Spain); B) Medentika 8500 Multi-Unit scan body® (Medentika GmbH, a Straumann Group, Hügelsheim, Germany); C) Elos Accurate Intra Oral Position Locator Kit Multi-unit Abutment NP/RP IO 2C-A® (Elos, Gothenburg, Sweden); D) IPD/AB-SR-01 scan body® (IPD Dental, Matarò, Barcelona, Spain).

data for each SB.

The RM standard tessellation language (STL) file was used to establish a geometric framework for the analysis of the inter-implant distances. The top surface of each PMC, screwed on a MUA, was designated as the uppermost z-plane. From this, the central axis of each PMC was determined. The z-plane was then translated 10 mm in the apical direction, thereby defining a base z-plane, which also served as the datum plane for each cylinder. The point located at the intersection between the base z-plane and the central axis of each PMC served as the origin point for subsequent spatial analysis. A linear distance was calculated using the Euclidean distance (inter-implant distance) between the origin points across all four MUAs.

This methodology was replicated across all experimental scans for each scanning system under evaluation. For each scan, the base of the SB was aligned to define the z-plane at the datum, and the central axis of each SB was determined accordingly. The intersection of each SB's axis with the z-plane at the datum was used to calculate the inter-implant distance among the four SBs in the same manner as the reference model.

Deviation analysis was conducted by comparing the inter-implant distance measurements of each test scan against those from the RM. The inter-implant distance, or Euclidean Distance, refers to the distance between the centers of two implants, which is depicted as the origin point at the intersection of the SB axis and z-plane. As shown in Fig. 3 the inter-implant distances between 4 MUA positions were computed. Specifically, the 6 inter-implant distances were measured, corresponding to the different implant pairs. The comparisons calculated between the experimental scan and RM enabled the evaluation of trueness and precision of the different scanning systems.

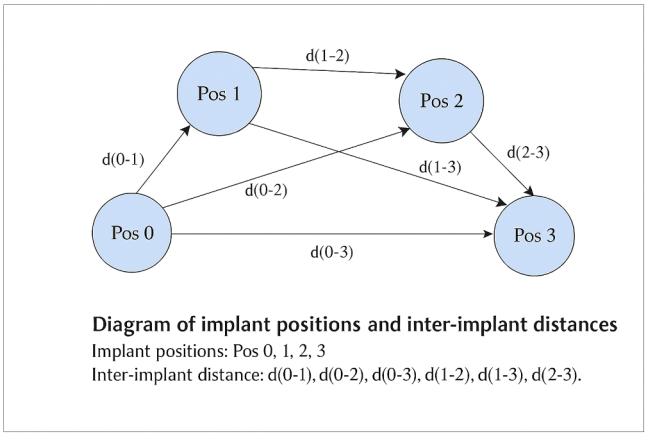

Fig. 3. Deviation analysis was conducted by comparing the inter-implant distance (i.e. the distance between the centres of two implants, which is depicted as the origin point at the intersection of the SB axis and z-plane measurements) of each test scan, against those from the RM. Specifically, six inter-implant distances were measured, corresponding to the different implant pairs.

The outcome variables were the trueness and precision of the inter-implant distances with the different systems. Trueness refers to the value to which measurements from the experimental scan correspond to

the RM. It is defined as the mean linear discrepancies between the reference model and each of the experimental scans. A lower mean deviation indicates higher trueness, reflecting conformity with the true geometry of the RM. Precision highlights the consistency or reproducibility of the measurements within each scanning group. It is defined as the linear deviation between each scan of the scanning group. High precision is characterised by minimal deviation amongst the scans, indicating that the system produces stable and repeatable results under the same scanning conditions. Together, trueness and precision provide a comprehensive assessment of each scanning group's performance.

2.3.1. The inter-implant distance

Each implant scan was aligned to a common coordinate system where Pos 0 (the first implant) served as the origin. The x, y, and z coordinates of each remaining implant (Pos 1, Pos 2, Pos 3) were measured relative to Pos 0, and deviations in linear distance were calculated for all six possible inter-implant pairs (d0–1, d0–2, d0–3, d1–2, d1–3, d2–3). The Euclidean distance (ED) values were extracted for each of the six inter-implant pairs [d(0–1), d(0–2), d(0–3), d(1–2), d(1–3), d(2–3)], as illustrated in Fig. 3. The deviation between each test scan and the reference model (RM) was calculated in micrometers (μm) along the three spatial axes (X, Y, Z) and as a combined 3D vector magnitude using the formula $\sqrt{(\Delta X^2 + \Delta Y^2 + \Delta Z^2)}$. These values were used to quantify both trueness (mean deviation from RM) and precision (standard deviation within repeated scans). The overall inter-implant distance discrepancies were then compared across the five systems (Nexus IOS®, DESS®, IPD®, Nobel Elos®, and Zimmer Medentika®) using one-way ANOVA with post-hoc Tukey analysis ($\alpha = 0.05$).

2.3.2. The point to point evaluation

The Point to Point evaluation compared the distances between centroids (implant datums) compared to the CMM. To calculate the linear point-to-point deviation in between the MUAs, the coordinate systems were superimposed and the deviation of the implant-abutment interface centers (inter implant distances) calculated via:

$$\Delta d = \sqrt[2]{(x_2 - x_1)^2 + (y_2 - y_1)^2 + (z_2 - z_1)^2}$$

With Δd= inter implant distance; x1,y1,z1= coordinates on the scans; x2,y2,z2= coordinates on the CMM).

Therefore, the point-to-point linear deviation between Nexus IOS® and Compatible Nobel MUA Scan bodies vs CMM data, were compared in order to see if there is a statistically significant difference in the XYZ axis. The in-pair linear deviations (Inter-implant distances) between Nexus IOS® vs CMM, Compatible SB Nobel MUA were compared in order to see if there is a statistically significant difference. There were 4 implant positions and 6 inter-implant distances for the all-on-4 reference implant case.

2.4. Statistical analysis

A descriptive analysis was first performed for each of the five scan systems, including the calculation of the mean, standard deviation, median, minimum and maximum values, as well as the 25th and 75th percentiles. To assess the precision of each system, the coefficient of variation (CV %) was calculated both per segment and overall.

To evaluate systematic differences between systems and segments, a repeated measures ANOVA was conducted separately for each of the four dependent variables: *overall deviation, ΔZ, ΔXY*, and *AVG XYZ*. In the model, the within-subject factor was the segment (i.e., the six inter-implant distances: 0–1, 0–2, 0–3, 1–2, 1–3, 2–3), and the between-subject factor was the scan system (Nexus IOS®, DESS®, IPD®, Nobel Elos®, Zimmer Medentika®).

This design allowed us to address the following questions:

1. Are there overall differences among scan systems?
2. Are there overall differences among segments/points?
3. For a given segment/point, do scan systems perform differently?

Mauchly's test was used to assess the assumption of sphericity. When this assumption was violated, the Greenhouse–Geisser correction was applied. Pairwise comparisons were explored through post hoc tests with Bonferroni correction.

A p-value <0.05 was considered statistically significant.

All analyses were conducted using IBM SPSS Statistics, version 30.

3. Results

For the dependent variable difference (mm) Nexus IOS® and DESS® had the lowest overall means and weren't significantly different from each other. However, Nexus IOS® had significantly lower values than all other systems and DESS®, from a statistically significant standpoint, performed better in terms of mean difference only when compared to Nobel Elos® (Fig. 4, Fig. 5).

Segments 0–2 and 0–3 appeared to have a significantly higher overall average than the other segments. The difference between them was not significant. Observing the differences between systems for the same measured distance, we observed that:

- for the 0–1 measurement, there was no significant difference between the systems.
- for the 0–2 measurement, we observed that the Nobel Elos® values were significantly higher than all other systems, and Nexus IOS® had significantly lower values than Zimmer Medentika®;
- in the 0–3 measurement, we observe that Nobel Elos® and Zimmer Medentika® had significantly higher values than DESS® and Nexus IOS®;
- in the 1–2 measurement, IPD® showed significantly higher values than all other systems, except Nobel Elos®.
- in the 1–3 measurement, there were no significant differences between the systems.
- in the 2–3 measurement, we observed that the IPD® values were significantly higher than those of DESS®, Nexus IOS®, and Zimmer Medentika®.

For ΔZ the system does not appear to be a significant between-factor (p-value=0.313), and there is no significant difference between the systems even when considering the points separately. Pairwise comparisons (Bonferroni-corrected) between the four points revealed some significant differences. ΔZ scores were significantly higher at 2 and 3 than at 1 ($p < .001$, respectively). However, at 4, scores significantly decreased compared to both 2 ($p < .001$) and 3 ($p < .001$), returning to levels comparable to 1 ($p = 1.000$). No significant differences were found between times 2 and 3.

For ΔXY is observed that the Nobel Elos® system values are significantly higher than those of Nexus IOS® and DESS®. Compared to Nexus IOS®, significantly higher values are also observed for IPD®. Pairwise comparisons (Bonferroni-corrected) between the four points revealed some significant differences. ΔXY scores were significantly higher at 1 and 4 than at 2 and 3 (p-value < 0.05). The values for 3 were significantly higher than those for 2 (p-value < 0.001). At 4, an increase in scores was again observed compared to both 2 ($p < .001$) and 3 ($p < .001$), returning to levels comparable to 1 ($p = 1.000$).

- For point 1 the value of Nobel Elos® is statistically significantly greater than the other systems, except for Zimmer Medentika®. Zimmer Medentika® has a significantly higher value than DESS® and Nexus IOS®.
- For point 2, there are no significant differences between the systems.
- For point 3, we observe that IPD® has significantly higher values than DESS®, Nexus IOS®, and Zimmer Medentika®. Nexus IOS® has a value significantly lower than DESS® and Nobel Elos®, too.

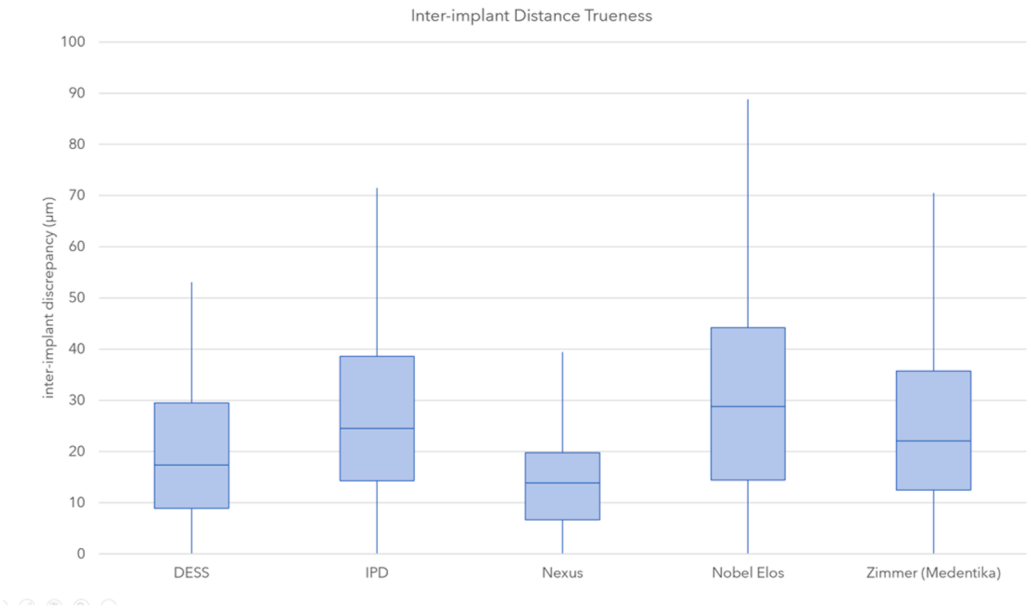

Fig. 4. Box plot illustrating inter-implant distance trueness across the five systems (DESS, IPD, Nobel Elos, Zimmer Medentika, and Nexus IOS). The plot represents the distribution of linear discrepancies (in µm) from the reference inter-implant distances. Each box shows the interquartile range (IQR), with the horizontal line indicating the median value. Whiskers denote the full range of deviations, reflecting system-specific dimensional accuracy and variability in full-arch implant scans.

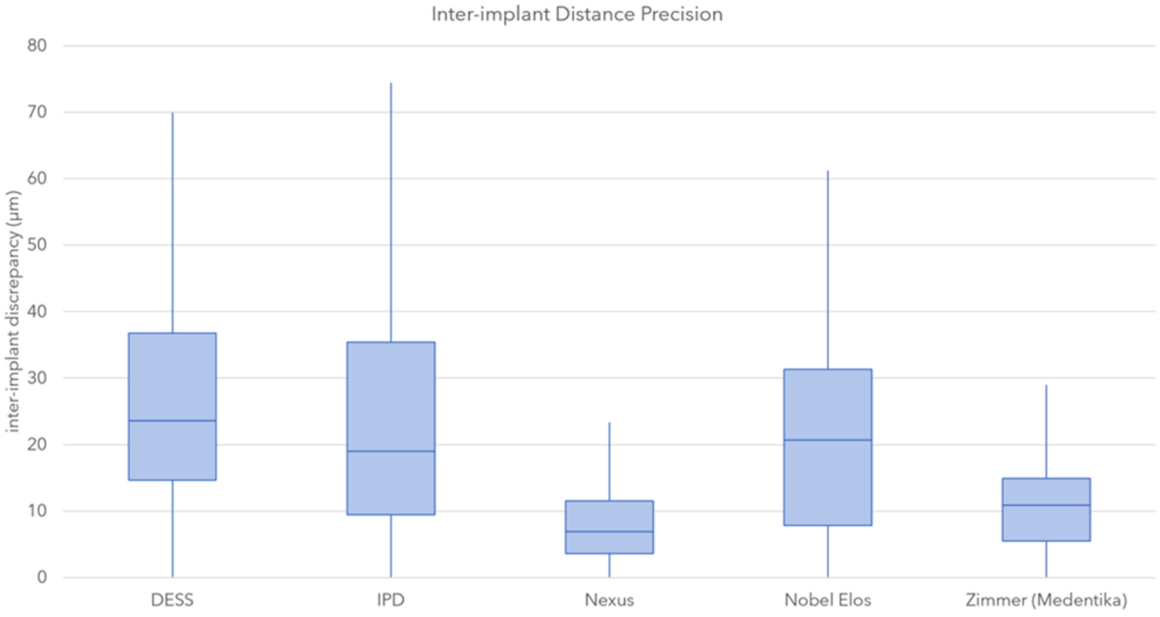

Fig. 5. Box plot illustrating inter-implant distance precision for the five systems. Precision is represented by the distribution of inter-implant linear discrepancies (µm) across repeated scans within each system. Narrower interquartile ranges and smaller overall spread indicate greater scan repeatability.

Zimmer Medentika® has a significantly lower value than all the other systems except for Nexus IOS®.
- In the 4-point, Nexus IOS® has a significantly lower value than Nobel Elos® and Zimmer Medentika®.

For ΔVGXYZ is observed that the values for the Nobel Elos® and IPD® systems are significantly higher compared to Nexus IOS®. The point that is statistically significantly different from the others is the second one, whose values show the lowest mean. The differences between systems for the same point show that:

- For point 1 the value of Nobel Elos® is statistically significantly greater than the other systems, except for Zimmer Medentika®. Zimmer Medentika® has a significantly higher value than DESS® and Nexus IOS®.
- For point 2, there are no significant differences between the systems.
- For point 3, we observe that IPD® has significantly higher values than DESS®, Nexus IOS®, and Zimmer Medentika®.
- In the 4-point, Nexus IOS® has a significantly lower value than Zimmer Medentika®.

4. Discussion

Achieving marginal integrity and a passive fit is essential for the long-term success of ISFDPs [41,42]. Marginal discrepancies between 10 and 100 µm are generally considered clinically acceptable; greater

misfits, however, may lead to biological complications such as peri-implant mucositis or peri-implantitis [42]. Although limited bone remodeling may compensate for minor strain in non-passive restorations [43], significant misfit increases the risk of mechanical failures, including screw loosening, framework fracture, ceramic chipping, and even implant loss [42,44,45].

In this *in vitro* comparative study, the Nexus IOS® system achieved the highest accuracy, with a median deviation of approximately 14 μm, a narrow interquartile range (IQR ~8–20 μm), and a maximum deviation below 40 μm, indicating strong consistency. The DESS® system ranked second (median ~16 μm; IQR ~8–30 μm; max >50 μm). IPD® and Zimmer Medentika® showed comparable median deviations (~22–24 μm) but broader IQRs (~15–38 μm), reflecting moderate variability. Nobel Elos® demonstrated the lowest accuracy, with a median exceeding 30 μm (IQR ~17–45 μm; max ~90 μm), indicating less consistent dimensional precision.

In terms of precision, Nexus IOS® again outperformed the other systems, showing the narrowest IQR (~5–10 μm) and minimal variation. Zimmer Medentika® also exhibited high repeatability (IQR ~8–16 μm), while DESS®, IPD®, and Nobel Elos® displayed wider spreads (IQRs ~15–40 μm). Even when differences in precision are not statistically significant, final ISFDP fit depends on the cumulative effect of scanning deviations and manufacturing tolerances, which can introduce gaps of 20–100 μm [46,47]. Thus, the superior accuracy observed with Nexus IOS® may be clinically relevant for minimizing misfit-related errors.

These findings align with those of Laureti et al. [48], who reported the highest trueness for Nexus IOS® compared with three horizontal and one vertical SB designs scanned with four IOS devices. Their trueness analysis based on root-mean-square (RMS) values confirmed the superior accuracy of Nexus IOS®. Similarly, a recent *in vitro* study [49] demonstrated that frameworks fabricated with Nexus IOS® SGs achieved superior passivity compared with those made using conventional SBs. Together, these results reinforce the system's dimensional reliability in full-arch implant scanning.

The present outcomes also corroborate previous clinical studies by Giglio et al. [50] and Klein et al. [40]. Klein et al. evaluated 37 ISFDPs fabricated with the Nexus IOS® system and observed excellent passive fit and marginal integrity, confirmed through the Sheffield test and radiographic assessment. Implant survival at one year was 100%, with only minor technical issues (8.1% incidence) and no major biological complications [40]. These findings mirror reports on full-arch zirconia restorations [51], where high survival rates and minimal prosthetic issues were recorded over 12–20 months, with only minor, non-intervention fractures [51]. Such results support the premise that optimal prosthetic fit and marginal adaptation minimize complications regardless of restorative material [44,48]. A recent systematic review further confirmed high survival and low complication rates in monolithic zirconia-based ISFDPs [44].

The Nexus IOS® system presents several advantages for full-arch implant scanning.

First, its horizontally oriented SGs of varying heights and lengths, positioned on MUAs, differ fundamentally from conventional vertically oriented SBs [40,46]. This horizontal configuration creates continuous overlap between adjacent SGs, ensuring an uninterrupted scan path and allowing all surfaces to be captured in a single, efficient pass. By minimizing inter-implant gaps and image overlap, it reduces stitching errors typically associated with multi-frame scans [40,46]. This concept supports findings by Imburgia et al. [20], who successfully produced 35 monolithic zirconia restorations using a continuous scan protocol linking SBs with thermoplastic resin. Similar *in vitro* studies by Ashraf et al. [33], Pradies et al. [52], and Pozzi et al. [53] confirmed that connecting SBs improves scanning accuracy.

Second, each Nexus IOS® SG has a unique geometry and dedicated digital library generated through AI-assisted calibration [40,46]. This process minimizes manufacturing tolerance errors documented with conventional SBs [22]. The AI algorithm analyzes the SG's geometric features across multiple planes, filtering low-quality scan data and aligning only the most reliable points with the library model [26]. This enhances implant position detection accuracy. The titanium SGs also ensure dimensional stability over time and resist deformation from sterilization, unlike polyether-ether-ketone (PEEK) components [54]. They are reusable without accuracy loss.

Third, the system's proprietary algorithm utilizes multiple SG facets to improve mesh-to-library alignment, minimizing discrepancies between digital and actual implant positions [40,46]. Deviations exceeding 20 μm per SB can cause clinically relevant misfits [26]; thus, reducing stitching and alignment errors directly enhances restoration precision.

Compared with SI workflows, Nexus IOS® is fully digital, eliminating the need for analog impressions. Relative to ASs, it simplifies clinical procedures by requiring only one intraoral scan, reducing chair time and patient appointments. In contrast to EPG, Nexus IOS® requires no additional hardware or complex data superimposition. Unlike IPG, currently compatible only with the Elite® IOS (Shining 3D, Hangzhou, China) [36,37], Nexus IOS® integrates with all major IOS devices.

Overall, the system's design may reduce intraoral scanning errors and enhance the predictability of full-arch workflows, enabling fabrication of restorations with improved fit, passivity, and precision—potentially within just two appointments. Nevertheless, certain limitations remain. The system is currently restricted to use on MUA connections and is incompatible with direct-to-implant scanning. Although not universally adaptable to all implant brands, it supports most major systems and common MUA platforms. Additionally, data processing is centralized through Osteon Medical, the exclusive manufacturer of final restorations. While this may limit flexibility, it ensures adherence to validated protocols and stringent quality control, supporting consistent precision and reproducibility.

This *in vitro* study also presents limitations: the Nexus IOS® SGs were compared with only a few conventional SBs; the sample size was limited; and all scans were performed by a single operator using one scanning strategy, with only one IOS. Therefore, further *in vitro* and clinical studies are required to confirm the promising outcomes observed with the Nexus IOS® system.

5. Conclusions

Within the limitations of this *in vitro* study, the Nexus IOS® SGs demonstrated the highest overall trueness and precision in the measurement of inter-implant linear deviations, outperforming conventional vertical SB systems. The Nexus IOS® consistently exhibited the lowest mean deviation and the narrowest IQR range, confirming its superior dimensional stability in FA implant scanning. The findings suggest that calibrated SG systems can effectively minimize distortion and variability commonly observed with traditional SBs, providing more predictable digital implant impressions. Such accuracy may translate clinically into improved passive fit of FA frameworks, reduced mechanical strain at the implant–abutment interface, and enhanced long-term prosthetic reliability. While these results are encouraging, further *in vivo* studies are warranted to validate the clinical performance of the Nexus IOS® system under dynamic intraoral conditions.

Abbreviations

FA: full-arch; SG: scan gauge; SB: scanbody; CMM: coordinate measuring machine; CAM: computer-assisted-manufacturing; IOS: Intraoral scanners; CAD: computer-assisted-design; CAM: vomputer-assisted-manufacturing; 3D: three-dimensional; SC: single crowns; FPD: fixed partial dentures; ISFDP: implant supported full-arch fixed dental prostheses; SI: solid index; AS: auxiliary system; EPG: extraoral photogrammetry; IPG: intraoral photogrammetry;; MUA: multi-unit-abutment; RM: reference model; PMC: precision made cylinder; STL: standard tesselletion language; CV: coefficient of variation; IQR:

interquartile range; RMS: root mean square; PEEK: polyether-ether-ketone.

Disclaimer

The materials in the present article belongs to the authors, therefore no conflict of interest related to this work is reported. Although Michael Klein is a consultant of Keystone Dental, this study was conducted independently and the authors did not receive any grant or material for the development of this research.

CRediT authorship contribution statement

Henriette Lerner: Writing – original draft, Visualization, Validation, Supervision, Software, Resources, Project administration, Methodology, Investigation, Funding acquisition, Formal analysis, Data curation, Conceptualization. **Paul Weigl:** Writing – review & editing, Visualization, Validation, Supervision, Software, Resources, Project administration. **Robert Sader:** Writing – review & editing, Visualization, Validation, Supervision, Software, Resources, Project administration. **Michael Klein:** Methodology, Investigation, Funding acquisition, Formal analysis, Data curation, Conceptualization. **Mariano A. Polack:** Writing – review & editing, Writing – original draft, Methodology, Investigation, Funding acquisition, Formal analysis, Data curation, Conceptualization. **Frank J. Tuminelli:** Writing – review & editing, Writing – original draft, Methodology, Investigation, Funding acquisition, Formal analysis, Data curation, Conceptualization.

Declaration of competing interest

The authors report no conflict of interest related to this study. The materials presented in the study belong to the authors, who have not received any grant or financial support for the preparation of the present research.

References

[1] F. Eggmann, M.B. Blatz, The core of digital dentistry: intraoral scanners, Compend. Contin. Educ. Dent. 45 (2024) 503–507.

[2] L.I. Abdulkarim, F.S.S. Alharamlah, R.M. Abubshait, D.A. Alotaibi, A.O. Abouonq, Impact of digital workflow integration on fixed prosthodontics: a review of advances and clinical outcomes, Cureus. 16 (2024) e72286, https://doi.org/10.7759/cureus.72286.

[3] M.S.N. Borges, G.G. de Carvalho, G.A. de Souza, K. Pintado-Palomino, B.N. de Freitas, C. Tirapelli, Does intraoral scanning influence the patient's view of dental restorations? A comparative study, Digital Dent. J. 1 (2025) 100004, https://doi.org/10.1016/j.ddj.2025.100004.

[4] G. Ruggiero, R. Sorrentino, P. Venezia, G. Luongo, F. Zarone, Qualitative aspects and minimum requirements of milling machines in digital dentistry: a narrative review, Digital Dent. J. 1 (2025) 100010, https://doi.org/10.1016/j.ddj.2025.100010.

[5] S. Khaw, X. Liu, A.B. Cameron, J.M. Aarts, J.J.E. Choi, Influence of temperature on the dimensional stability of DLP- and FDM-printed dental casts with different base designs, Digital Dent. J. 2 (2025) 100016, https://doi.org/10.1016/j.ddj.2025.100016.

[6] F. Mangano, G. Veronesi, Digital versus Analog procedures for the prosthetic restoration of single implants: a randomized controlled trial with 1 year of follow-up, Biomed. Res. Int. 2018 (2018) 5325032, https://doi.org/10.1155/2018/5325032.

[7] F. Mangano, B. Margiani, O. Admakin, A novel full-digital protocol (SCAN-PLAN-MAKE-DONE®) for the design and fabrication of implant-supported monolithic translucent zirconia crowns cemented on customized hybrid abutments: a retrospective clinical study on 25 patients, Int. J. Environ. Res. Public Health 16 (2019) 317, https://doi.org/10.3390/ijerph16030317.

[8] H. Lerner, J. Mouhyi, O. Admakin, F. Mangano, Artificial intelligence in fixed implant prosthodontics: a retrospective study of 106 implant-supported monolithic zirconia crowns inserted in the posterior jaws of 90 patients, BMC. Oral Health 20 (2020) 80, https://doi.org/10.1186/s12903-020-1062-4.

[9] S. Mühlemann, S.T. Lamperti, L. Stucki, C.H.F. Hämmerle, D.S. Thoma, Time efficiency and efficacy of a centralized computer-aided-design/computer-aided-manufacturing workflow for implant crown fabrication: a prospective controlled clinical study, J. Dent. 127 (2022) 104332, https://doi.org/10.1016/j.jdent.2022.104332.

[10] D. Guo, S. Mühlemann, S. Pan, Y. Zhou, R.E. Jung, A double-blind randomized within-subject study to evaluate clinical applicability of four digital workflows for the fabrication of posterior single implant crown, Clin. Oral Implants Res. 34 (2023) 1319–1329, https://doi.org/10.1111/clr.14171.

[11] P. Pontevedra, C. Lopez-Suarez, V. Rodriguez, J. Pelaez, M.J. Suarez, Randomized clinical trial comparing monolithic and veneered zirconia three-unit posterior fixed partial dentures in a complete digital flow: three-year follow-up, Clin. Oral Investig. 26 (2022) 4327–4335, https://doi.org/10.1007/s00784-022-04396-y.

[12] F.G. Mangano, K.R. Yang, H. Lerner, T. Porrà, L.G. Khachatryan, I.D. Gordienko, O. Admakin, 3D-printed short-span hybrid composite implant-supported restorations fabricated through tilting stereolithography: a retrospective clinical study on 85 patients with 1 year of follow-up, J. Dent. 147 (2024) 105095, https://doi.org/10.1016/j.jdent.2024.105095.

[13] J. Mouhyi, M. Salama, A. Mouhyi, H. Lerner, B. Margiani, C. Mangano, A novel coded healing abutment for a simplified digital workflow: a retrospective clinical study on 103 patients with a one year follow-up, J. Dent. 152 (2025) 105465, https://doi.org/10.1016/j.jdent.2024.105465.

[14] J. Ma, B. Zhang, H. Song, D. Wu, T. Song, Accuracy of digital implant impressions obtained using intraoral scanners: a systematic review and meta-analysis of in vivo studies, Int. J. ImPlant Dent. 9 (2023) 48, https://doi.org/10.1186/s40729-023-00517-8.

[15] N. Joensahakij, P. Serichetaphongse, W. Chengprapakorn, The accuracy of conventional versus digital (intraoral scanner or photogrammetry) impression techniques in full-arch implant-supported prostheses: a systematic review, Evid. Based. Dent. 25 (2024) 216–217, https://doi.org/10.1038/s41432-024-01045-z.

[16] Y.J. Zhang, J.Y. Shi, S.J. Qian, S.C. Qiao, H.C. Lai, Accuracy of full-arch digital implant impressions taken using intraoral scanners and related variables: a systematic review, Int. J. Oral Implantol. (Berl) 14 (2021) 157–179.

[17] V. Vitai, A. Nemeth, E. Solyom, L.M. Czumbel, B. Szabo, R. Fazekas, G. Gerber, P. Hegyi, P. Hermann, J. Borbely, Evaluation of the accuracy of intraoral scanners for complete-arch scanning: a systematic review and network meta-analysis, J. Dent. 137 (2023) 104636, https://doi.org/10.1016/j.jdent.2023.104636.

[18] F.G. Mangano, O. Admakin, M. Bonacina, H. Lerner, V. Rutkunas, C. Mangano, Trueness of 12 intraoral scanners in the full-arch implant impression: a comparative in vitro study, BMC. Oral Health 20 (2020) 263, https://doi.org/10.1186/s12903-020-01254-9.

[19] S. Aneakgerawat, W. Narkbuakaew, W. Aunmeungtong, P. Khongkhunthian, A comparative study of the accuracy between conventional and digital impressions in different implant angulations and depths, Digital Dent. J. 1 (2025) 100009, https://doi.org/10.1016/j.ddj.2025.100009.

[20] M. Imburgia, J. Kois, E. Marino, H. Lerner, F.G. Mangano, Continuous scan strategy (CSS): a novel technique to improve the accuracy of intraoral digital impressions, Eur. J. Prosthodont. Restor. Dent. 28 (2020) 128–141, https://doi.org/10.1922/EJPRD_2105Imburgia14.

[21] A. Schmidt, B. Wöstmann, M.A. Schlenz, Accuracy of digital implant impressions in clinical studies: a systematic review, Clin. Oral Implants Res. 33 (2022) 573–585, https://doi.org/10.1111/clr.13951.

[22] H. Lerner, K. Nagy, F. Luongo, G. Luongo, O. Admakin, F.G. Mangano, Tolerances in the production of six different implant scanbodies: a comparative study, Int. J. Prosthodont. 34 (2021) 591–599, https://doi.org/10.11607/ijp.7379.

[23] Y. Kim, D. Kim, H. Son, S.J. Hong, H.S. KIm, A. Pae, Effect of number and angulation of implants on accuracy of digital impression in completely edentulous arch, Int. J. Prosthodont. (2025 Feb 6), https://doi.org/10.11607/ijp.9174. Online ahead of print.

[24] M. Revilla-León, R. Aragoneses, E.M. Arroyo Valverde, M. Gómez-Polo, J.C. Kois, Classification of scanning errors of digital scans recorded by using intraoral scanners, J. Esthet. Restor. Dent. 37 (2025) 1363–1371, https://doi.org/10.1111/jerd.13419.

[25] F.D. Boz, K. Akça, A retrospective cohort study on scan quality of implant scanbodies matched with CAD libraries, Clin. ImPlant Dent. Relat. Res. 27 (2025) e70017, https://doi.org/10.1111/cid.70017.

[26] U. Hauschild, H. Lerner, P. Weigl, T. Porrà, O. Admakin, F.G. Mangano, Effects of the intraoral scanner and implant library on the trueness of digital impressions in the full-arch implant scan: a comparative in vitro study, J. Dent. 150 (2024) 105336, https://doi.org/10.1016/j.jdent.2024.105336.

[27] F.G. Mangano, M. Bonacina, F. Mandelli, F. Marchiori, Solid index versus intraoral scanners in the full-arch implant impression: in vitro trueness evaluation, BMC. Res. Notes. 13 (2020) 504, https://doi.org/10.1186/s13104-020-05353-2.

[28] F.G. Mangano, F. Marchiori, C. Mangano, O. Admakin, Solid index and reverse implant library for the fabrication of a bar for overdenture: a proof of concept, Int. J. Comput. Dent. 24 (2021) 331–343, https://doi.org/10.3290/j.ijcd.b1999901.

[29] F. Mandelli, A. Zaetta, A. Cucchi, F.G. Mangano, Solid index impression protocol: a hybrid workflow for high accuracy and passive fit of full-arch implant-supported restorations, Int. J. Comput. Dent. 23 (2020) 161–181.

[30] F. Llansana, S. Guirao, J.C. Kois, M. Revilla-León, Calibrated splinting framework for complete arch intraoral implant digital scans manufactured by combining milled and additively manufacturing technologies: a dental technique, J. Prosthet. Dent. 132 (2024) 680–686, https://doi.org/10.1016/j.prosdent.2022.08.031.

[31] M. Revilla-León, A.B. Barmak, A. Lanis, J.C. Kois, Influence of connected and nonconnected calibrated frameworks on the accuracy of complete arch implant scans obtained by using four intraoral scanners, a desktop scanner, and a photogrammetry system, J. Prosthet. Dent. (2024 Mar 4), https://doi.org/10.1016/j.prosdent.2024.01.017. S0022-3913(24)00048-9Online ahead of print.

[32] F. Rustichini, R. Romolini, M.C. Salmi, L. Gennai, F. Vermigli, F.G. Mangano, Implant-supported full-arch fixed dental prostheses manufactured through a direct digital workflow using a calibrated splinting framework: a retrospective clinical study, J. Dent. 154 (2025) 105605, https://doi.org/10.1016/j.jdent.2025.105605.

[33] Y. Ashraf, A. El Fadl, A. Hamdy, K. Ebeid, Effect of different intraoral scanners and scanbody splinting on accuracy of scanning implant-supported full arch fixed prosthesis, J. Esthet. Restor. Dent. 35 (2023) 1257–1263, https://doi.org/10.1111/jerd.13070.
[34] J. Cheng, H. Zhang, H. Liu, J. Li, H.L. Wang, X. Tao, Accuracy of edentulous full-arch implant impression: an in vitro comparison between conventional impression, intraoral scan with and without splinting, and photogrammetry, Clin. Oral Implants Res. 35 (2024) 560–572, https://doi.org/10.1111/clr.14252.
[35] J. Conejo, M. Ordway, T.H. Yoo, H.P. Fraiman, P.J. Atria, L. Retana, M.B. Blatz, L. S. Prott, In vitro comparison between complete-arch implant supported frameworks using intraoral scanning and photogrammetry, Int. J. Prosthodont. (2025 May 20), https://doi.org/10.11607/ijp.9363. Online ahead of print.
[36] J. Brakoč, A. Todorović, F.G. Mangano, M. Glišić, M. Šćepanović, Accuracy of intraoral photogrammetry versus direct digital implant impressions in the fully edentulous lower jaw: an in vitro study, J. Dent. 156 (2025) 105654, https://doi.org/10.1016/j.jdent.2025.105654.
[37] A.K. Eldabe, D. Adel-Khattab, K.H. Botros, Accuracy of intraoral photogrammetry in complete arch digital implant scanning: an in vivo prospective comparative study, J. Prosthet. Dent. (2025 Apr 18), https://doi.org/10.1016/j.prosdent.2025.03.041. S0022-3913(25)00294-XOnline ahead of print.
[38] M. Khalili, Enhancing precision and efficiency in fabricating complete arch screw-retained implant prosthesis: a clinical case report utilizing the Nexus iOS scan gauge system, J. Oral Implantol. 50 (2024) 160–165, https://doi.org/10.1563/aaid-joi-D-24-00019.
[39] M. Jeong, S. Ishikawa-Nagai, J.D. Lee, S.J. Lee, Accuracy of impression scan bodies for complete arch fixed implant-supported restorations, J. Prosthet. Dent. 134 (2025) 425–432, https://doi.org/10.1016/j.prosdent.2023.11.015.
[40] M. Klein, F.J. Tuminelli, A. Sallustio, G.D. Giglio, H. Lerner, R.W. Berg, A. Waltuch, Full-arch restoration with the NEXUS IOS® system: a retrospective clinical evaluation of 37 restorations after a one year of follow-up, J. Dent. 139 (2023) 104741, https://doi.org/10.1016/j.jdent.2023.104741.
[41] J. Katsoulis, T. Takeichi, A. Sol Gaviria, P. Lukas, K. Katsoulis, Misfit of implant prostheses and its impact on clinical outcomes. Definition, assessment and a systematic review of the literature, Eur. J. Oral Implantol. 10 (Suppl) (2017) 121–138.
[42] S. Al-Tarawneh, G. Thalji, D. Shonberg, L. Fayz, L. Cooper, Retrospective cohort evaluation of full-arch zirconia implant-supported fixed prostheses, Int. J. Oral Maxillofac. Implants 38 (2023) 381–390, https://doi.org/10.11607/jomi.10022.
[43] M. Karl, T.D. Taylor, Bone adaptation induced by non-passively fitting implant superstructures: a randomized clinical trial, Int. J. Oral Maxillofac. Implants 31 (2016) 369–375, https://doi.org/10.11607/jomi.4331.
[44] S. Al-Tarawneh, G. Thalji, L. Cooper, Full-arch implant-supported monolithic zirconia fixed dental prostheses: an updated systematic review, Int. J. Oral Implantol. 14 (2021) 13–22.
[45] F. Tirone, S. Salzano, E. Rolando, D.A. Pirja, D. Rodi, Relation between CAD dimensional parameters and framework fracture in zirconia full arch implant rehabilitation: an observational cohort study, J. Dent. 160 (2025 May 24) 105851, https://doi.org/10.1016/j.jdent.2025.105851. Online ahead of print.
[46] A. Pozzi, L. Arcuri, P. Carosi, A. Laureti, J. Londono, H.L. Wang, Photogrammetry versus intraoral scanning in complete-arch digital implant impression: a systematic review and meta-analysis, Clin. ImPlant Dent. Relat. Res. 27 (2025) e70059, https://doi.org/10.1111/cid.70059.
[47] A. Ortorp, T. Jemt, T. Bäck, T. Jälevik, Comparisons of precision of fit between cast and CNC-milled titanium implant frameworks for the edentulous mandible, Int. J. Prosthodont. 16 (2003) 194–200.
[48] A. Laureti, T. Marques, J. Pitta, V. Fehmer, I. Sailer, A. Pozzi, L. Azevedo, Influence of horizontal intraoral scan bodies on the trueness of digital impressions for complete-arch prostheses on four implants: an In vitro evaluation, Clin. Oral Implants Res. 36 (2025) 1287–1295, https://doi.org/10.1111/clr.70001. Epub 2025 Jul 18.
[49] S. Kerzhner, H.C. Lin, F. Tuminelli, Passivity of complete arch implant-supported fixed dental prostheses fabricated using a scan gauge system and conventional scan bodies: an in vitro study, J. Prosthodont. (2025 Jun 14), https://doi.org/10.1111/jopr.14079. Online ahead of print.
[50] G.D. Giglio, A.B. Giglio, D.P. Tarnow, A paradigm shift using scan bodies to record the position of a complete arch of implants in a digital workflow, Int. J. Periodontics Restorative Dent. 44 (2024) 115–126, https://doi.org/10.11607/prd.6733.
[51] E. Mijiritsky, A. Elad, R. Krausz, V. Ivanova, S. Zlatev, Clinical performance of full-arch implant-supported fixed restorations made of monolithic zirconia luted to a titanium bar: a retrospective study with a mean follow-up of 16 months, J. Dent. 137 (2023) 104675, https://doi.org/10.1016/j.jdent.2023.104675.
[52] I. García-Martínez, C. Zarauz, B. Morejon, A. Ferreiroa, G. Pradíes, Influence of customized over-scan body rings on the intraoral scanning effectiveness of a multiple implant edentulous mandibular model, J. Dent. 122 (2022) 104095, https://doi.org/10.1016/j.jdent.2022.104095.
[53] A. Pozzi, L. Arcuri, F. Lio, A. Papa, A. Nardi, J. Londono, Accuracy of complete-arch digital implant impression with or without scanbody splinting: an in vitro study, J. Dent. 119 (2022) 104072, https://doi.org/10.1016/j.jdent.2022.104072.
[54] E. Diker, H. Terzioglu, D.N.M. Gouveia, M.B. Donmez, J. Seidt, B. Yilmaz, Effect of material type, torque value, and sterilization on linear displacements of a scan body: an in vitro study, Clin. ImPlant Dent. Relat. Res. 25 (2023) 419–425, https://doi.org/10.1111/cid.13187.